# Elastic Dispersion and Attenuation in Fully Saturated Sandstones: Role of Mineral Content, Porosity, and Pressures

Lucas Pimienta, Jan V M Borgomano, Jérôme Fortin, Yves Guéguen

AGU PUBLICATIONS

JGR

Journal of Geophysical Research: Solid Earth

RESEARCH ARTICLE
10.1002/2017JB014645

Special Section:
Seismic and Micro-Seismic Signature of Fluids in Rocks: Bridging the Scale Gap

# Elastic Dispersion and Attenuation in Fully Saturated Sandstones: Role of Mineral Content, Porosity, and Pressures

**Lucas Pimienta**[1,2], **Jan V. M. Borgomano**[1], **Jérôme Fortin**[1], **and Yves Guéguen**[1]

[1]Laboratoire de Géologie de l'ENS - PSL Research University - UMR8538 du CNRS, Paris, France, [2]Laboratory of Experimental Rock Mechanics, Ecole Polytechnique Fédérale de Lausanne, Lausanne, Switzerland

**Key Points:**
- Dispersions and attenuations over seismic frequency range in fluid-saturated sandstones
- Clear observation of the Biot-Gardner flow for all samples
- Different behavior in the high-frequency range for the different sandstones

**Correspondence to:**
L. Pimienta,
lucas.pimienta@epfl.ch

**Citation:**
Pimienta, L., Borgomano, J. V. M., Fortin, J., & Guéguen, Y. (2017). Elastic dispersion and attenuation in fully saturated sandstones: Role of mineral content, porosity, and pressures. *Journal of Geophysical Research: Solid Earth*, *122*, 9950–9965. https://doi.org/10.1002/2017JB014645

Received 30 JUN 2017
Accepted 2 NOV 2017
Accepted article online 20 NOV 2017
Published online 29 DEC 2017



**Abstract** Because measuring the frequency dependence of elastic properties in the laboratory is a technical challenge, not enough experimental data exist to test the existing theories. We report measurements of three fluid-saturated sandstones over a broad frequency band: Wilkenson, Berea, and Bentheim sandstones. Those sandstones samples, chosen for their variable porosities and mineral content, are saturated by fluids of varying viscosities. The samples elastic response (Young's modulus and Poisson's ratio) and hydraulic response (fluid flow out of the sample) are measured as a function of frequency. Large dispersion and attenuation phenomena are observed over the investigated frequency range. For all samples, the variation at lowest frequency relates to a large fluid flow directly measured out of the rock samples. These are the cause (i.e., fluid flow) and consequence (i.e., dispersion/attenuation) of the transition between drained and undrained regimes. Consistently, the characteristic frequency correlates with permeability for each sandstone. Beyond this frequency, a second variation is observed for all samples, but the rocks behave differently. For Berea sandstone, an onset of dispersion/attenuation is expected from both Young's modulus and Poisson's ratio at highest frequency. For Bentheim and Wilkenson sandstones, however, only Young's modulus shows dispersion/attenuation phenomena. For Wilkenson sandstone, the viscoelastic-like dispersion/attenuation response is interpreted as squirt flow. For Bentheim sandstone, the second effect does not fully follow such response, which could be due to a lower accuracy in the measured attenuation or to the occurence of another physical effect in this rock sample.

**Plain Language Summary** Field seismic is a powerful tool to investigate materials placed in locations where the eye cannot reach. From the measured elastic properties, one infers the rocks and saturating fluids at depths. This tool, however, relies on the understanding of the waves propagation through a given rock, in which knowledge is usually acquired from measurements in the laboratory. When comparing laboratory to field measurements, one major factor is the frequency of the wave traveling through the medium: at the megahertz in the laboratory, and below the kilohertz at the field scale. Our work aims at investigating experimentally the frequency dependence of the elastic properties in fluid-saturated sandstones. We show that, if the pore fluid pressure is large, the dispersion/attenuation effects over the frequency range can be very large: large differences in elastic properties are expected if the same rock is measured in the lab or on the field. Separating the different physical effects, we show that two main phenomena occur in fluid-saturated sandstones.

## 1. Introduction

When interpreting seismic data obtained at the field scale, accounting for the frequency dependence of the elastic wave velocities is a major challenge. Indeed, porous crustal rocks are known to be dispersive media. Their elastic properties are frequency dependent. In the upper crust, elastic dispersion and attenuation in fluid-saturated sedimentary rocks are expected to originate from fluid flow at different scales (Biot, 1941; Cleary, 1978; Mavko et al., 1979; Müller et al., 2010; O'Connell & Budiansky, 1977). As detailed in Müller et al. (2010), various theories have been developed to describe those different mechanisms. In partially saturated rocks, several mechanisms are expected to occur (e.g., Amalokwu et al., 2017; Chapman et al., 2016; Müller et al., 2010; Papageorgiou et al., 2016; Tisato et al., 2015). In fully saturated homogeneous rocks, only two mechanisms (Cleary, 1978; Gardner, 1962; Mavko et al., 1979; O'Connell & Budiansky, 1977) are expected

to occur over the allowed frequency range (e.g., Adelinet et al., 2010; Fortin et al., 2014; Sarout, 2012): the drained/undrained and undrained/unrelaxed (or "squirt flow") transitions, which separate the three distinct drained, undrained, and unrelaxed elastic regimes. Yet such conclusion relies on a very limited amount of data acquired on very few rock types.

Despite the technical complexity of measuring such effects in the laboratory, different teams aimed at investigating the frequency dependence of elastic properties in rocks using different methodologies (see Subramaniyan et al., 2014, and references therein). Under the lead of Spencer (1981), Jackson and Paterson (1987), and Batzle et al. (2001), the forced oscillation method, allowing measurements over a wide frequency range and under varying confining pressure, was shown promising and faced important technical advances over the last decade (e.g., Adelinet et al., 2010; Fortin et al., 2014; Madonna & Tisato, 2013; Mikhaltsevitch et al., 2014; Pimienta, Fortin, Borgomano, et al., 2016; Spencer & Shine, 2016; Szewczyk et al., 2016; Tisato & Madonna, 2012). The aim of most teams was in particular to investigate the squirt flow phenomenon (O'Connell & Budiansky, 1977; Mavko et al., 1979), responsible for inducing a transition from the undrained to the unrelaxed regime. For this purpose, most teams applied experimental undrained condition on the rock sample in order to investigate effects beyond the undrained regime. Several authors (e.g., Mikhaltsevitch et al., 2014, 2015, 2016b; Pimienta, Fortin, & Guéguen, 2015b, 2016; Pimienta, Fortin, Borgomano, et al., 2016; Spencer & Shine, 2016; Subramaniyan et al., 2015) interpreted the measured dispersion and attenuation in terms of squirt flow. Consistent with squirt flow theory, the observed dispersion/attenuation effect depends both on frequency and fluid viscosity.

Several experimental artifacts need, however, to be accounted for (e.g., Dunn, 1987; Gardner, 1962; Pimienta, Borgomano, et al., 2016). In the experimental methodology usually chosen (e.g., Batzle et al., 2006; Madonna & Tisato, 2013; Mikhaltsevitch et al., 2014; Tisato & Madonna, 2012), a valve is placed at the nearest of the rock sample to obtain experimental undrained conditions. However, a pure nil dead volume can seldom be achieved experimentally. As discussed by Pimienta, Borgomano, et al. (2016), the existence of a small but nonzero dead volume implies that the sample will not be purely undrained. In that case, the measured effect could be the Biot-Gardner effect (i.e., drained/undrained transition). This observation has long-reaching consequences when interpreting laboratory data on dispersion and attenuation in fluid-saturated rocks. To counter this limit, a new methodology has been designed at ENS (Pimienta, Fortin, & Guéguen, 2015a) in which a large dead volume is maintained at both ends of the sample. Using this approach, the drained/undrained transition has been evidenced (Pimienta, Fortin, & Guéguen, 2015a, 2015b). When a second frequency effect is measured at higher frequencies, with no fluid flow out of the sample, it can be safely interpreted as the undrained/unrelaxed transition (Pimienta, Fortin, & Guéguen, 2015b, 2016).

Those two transitions were documented only in two quartz-pure Fontainebleau sandstones of low porosity (e.g., Pimienta, Fortin, Borgomano, et al., 2016). As sandstones found in the nature are seldom clean (i.e., quartz pure) and can cover a broad range in porosity, this work reports measurement of dispersion and attenuation in three sandstone samples ranging in porosity and mineral content. First, the experimental method and the samples mineralogy and microstructure are described. Then, the frequency-dependent properties are reported for different effective confining pressures. Ultimately, comparing this data set with previous ones, interpretations are suggested and discussed.

## 2. Experimental Setup and Rock Samples

### 2.1. Experimental Setup

The experimental setup used for the study is an oil confining cell equipped of a maneuverable axial piston, allowing to apply pure confining pressures up to $P_c = 300$ MPa and deviatoric stress up to $\sigma_{ax} = 1,000$ MPa (Fortin et al., 2007). Two setups can be used: (i) Bulk modulus and its intrinsic dissipation are measured from pure hydrostatic oscillations by lifting the piston (e.g., Adelinet et al., 2010; Borgomano et al., 2017; David et al., 2013; Pimienta, Fortin, & Guéguen, 2015a); (2) Young's modulus and Poisson's ratio (and their intrinsic dissipations) are measured from axial stress oscillations by shifting down the piston (Borgomano et al., 2017; Pimienta, Fortin, & Guéguen, 2015b, 2016; Riviere et al., 2016). The piston is equipped with a piezoelectric actuator ***PI piezoceramics*** able to apply small axial stress oscillations at frequencies from 1 mHz up to 100 Hz. All rock samples are equipped with three couples of radial and axial strain gages. The gages are glued on the cylindrical surface, at the sample center. For this study, the confining pressure range chosen did not exceed

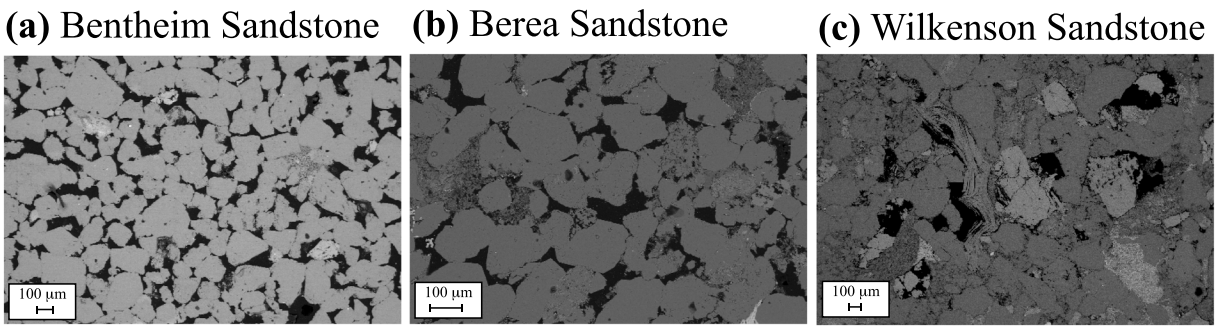


**Figure 1.** Scanning electron microscopy (SEM) images of thin sections of the (a) Bentheim sandstone, (b) Berea sandstone, and (c) Wilkenson sandstone. From the different gray levels, the denser materials are brighter as compared to the less dense ones. Quartz crystals dominantly appear as bright grains. For Berea and Bentheim sandstones, open grain contacts are observed. For Wilkenson sandstone, microcracked grains are also observed.

$P_c = 32$ MPa that is the blocking pressure for the actuator. Axial stress was kept to a minimum in order to avoid an effect of pressure-induced anisotropy on the measurements (Pimienta, Fortin, & Guéguen, 2015b). In the present contribution, Young's modulus $E$ and Poisson's ratio $\nu$ as well as their related dissipation coefficients are investigated. $E$ and $\nu$ are obtained from linear regression between axial stress and axial strain and between radial strain and axial strain, respectively. Their related dissipations, $Q_E^{-1}$ and $Q_\nu^{-1}$, are obtained from the tangent of the signal phase of those two end-members (e.g., Pimienta, Fortin, & Guéguen, 2016).

The pore fluid setup and procedure have been described in Pimienta, Fortin, and Guéguen (2015a). The fluid tubing is linked to a ***Quizix*** pump, able to deliver pressures in the range of [0;10] MPa. The fluid line can be either opened (i.e., drained conditions) or closed (i.e., experimentally undrained conditions) thanks to two valves situated at both sides of the sample. The total dead volume, at both ends of the sample, has been measured to be 6.6 mL. A pore pressure sensor is introduced in this dead volume. When changing confining pressures, the valves are opened to maintain a constant pore fluid pressure, and the sample is drained. When the measurement begins, the valves are closed and pore pressure variations are measured.

All samples are measured under both dry and liquid-saturated conditions. However, the liquid chosen differs for the rock samples: (i) Bentheim sandstone is measured under glycerine saturation, (ii) Wilkenson sandstone is measured under water saturation, and (iii) Berea sandstone is measured under saturation of glycerine and a water-glycerine mixture. To ascertain the repeatability of the measurements under water-glycerine saturation and investigate boundary effects, the sample is measured twice, that is, it is water saturated and dried after the first measurement then saturated again by the water-glycerine mixture. For the second measurement, the sample is equipped differently. Two strain gages are glued at the sample center, and two strain gages are glued near the bottom end platen to investigate boundary effects. More information is given in the section 5.

### 2.2. Rock Samples

The three sandstones investigated are Wilkenson, Bentheim, and Berea sandstones. Wilkenson sandstone is a low porosity (about 9% porosity) sandstone, with a quartz content of about 50% (Duda & Renner, 2013). Berea sandstone is a reference in the rock mechanics and rock (e.g., Christensen & Wang, 1985; Hart & Wang, 2010; Mavko & Vanorio, 2010; Pagoulatos & Sondergeld, 2004; Pimienta, Borgomano, et al., 2016; Prasad & Manghnani, 1997; Sayers et al., 1990; Spencer & Shine, 2016; Tao et al., 1995). Samples from this rock have porosities ranging from 17% to 23% and a quartz content ranging from 75% to 95% (Pimienta et al., 2014). Bentheim sandstone is a quartz-rich sandstone also used as a reference rock (e.g., Blöcher et al., 2014; Louis et al., 2005; Klein et al., 2001; Pimienta et al., 2017; Vajdova et al., 2004), with a porosity is in the range of 20% up to 25%. All three rock samples are documented to be isotropic and homogeneous at the sample scale, thus allowing for a good applicability of the method tested in this contribution.

As qualitatively shown from the SEM images (Figure 1), the selected samples cover a large porosity range (i.e., from about 10% up to 25%) and a wide range in mineral content (i.e., from about 50% up to 98% in quartz). Figure 2 shows the variability from one sample to the other: (i) Bentheim sandstone is almost quartz pure, showing only traces of feldspars; (ii) Berea sandstone shows presence of feldspars, present as inclusions in a quartz-dominated rock matrix; and (iii) Wilkenson sandstone shows a large quantity of feldspars and aluminosilicate minerals. From processing the various images acquired using ***ImageJ*** free software allows

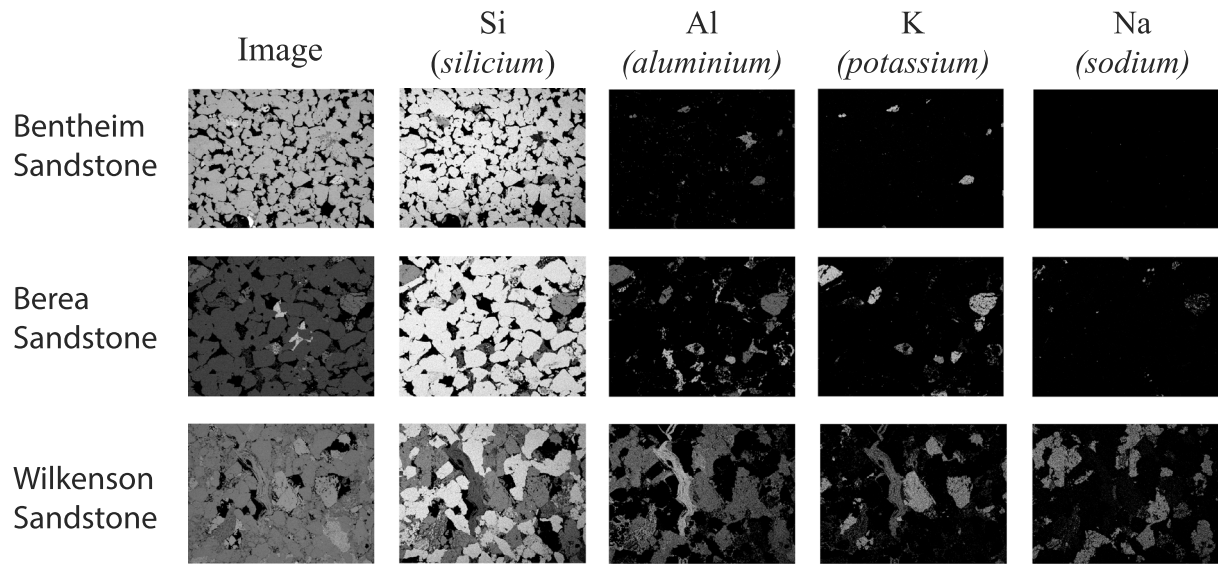


**Figure 2.** Energy dispersion spectrometry (EDS-SEM) image on the same thin sections as in Figure (1), showing the different atoms and their localization in the thin section of the rock sample.

to infer the approximate mineral content (Table 1). From the thin section, Wilkenson, Berea, and Bentheim sandstone samples have, respectively, (i) a quartz content of about 51%, 82%, and 98% and (ii) a porosity of about 10%, 22%, and 25%. A good consistency is obtained with literature data and with the three weighting method, leading to porosities of 9.1%, 19.2%, and 24.8%, respectively.

## 3. Results

### 3.1. Physical Properties of the Sandstones

#### 3.1.1. Permeability and Elastic Properties

For the three rock samples, permeability is measured as a function of Terzaghi effective pressure ($P_{eff}$). Moreover, the variation in volumetric strain of the sample is also recorded for characterization purposes. For comparison, we also report the permeability and volumetric strain on the two Fontainebleau sandstones investigated in Pimienta, Fortin, and Guéguen (2015b). The dependence of these two properties on $P_{eff}$ is reported in Figure 3.

The samples permeability (Figure 3a) range over 5 orders of magnitude, from about $10^{-18}$ m$^2$ for Wilkenson sandstone up to $2\times10^{-13}$ m$^2$ for Bentheim sandstone and exhibit varying dependences to confining pressure. The less permeable Wilkenson sandstone has a permeability that decreases from about $5\times10^{-18}$ m$^2$ down to $1\times10^{-18}$ m$^2$ as $P_{eff}$ increases from 1 to 30 MPa. The permeabilities of Berea sandstone (i.e., $2\times10^{-14}$ m$^2$) and Bentheim (i.e., $5\times10^{-13}$ m$^2$) sandstones are constant with pressure. The two Fontainebleau sandstones from Pimienta, Fortin, and Guéguen (2015b) appear to be in between these two extremes, with permeabilities of about $5\times10^{-15}$ m$^2$ and $1\times10^{-14}$ m$^2$, and with a slight dependence on $P_{eff}$.

**Table 1**
*Grain Size, Porosity, and Content in Elements From the SEM-EDS Images*

| Sandstone | Grain size (μm) | $\phi$ (%) | Quartz (%) | Al (%) | Ca (%) | Fe (%) | K (%) | Mg (%) | Na (%) |
|---|---|---|---|---|---|---|---|---|---|
| Bentheim | 150 | 25.09 | 97.87 | 2.88 | 0.02 | 0.05 | 1.13 | 0.07 | 0.17 |
| Berea | 100 | 21.69 | 81.71 | 9.35 | 0.27 | 0.54 | 6.18 | 2.88 | 1.81 |
| Wilkenson | 400 | 10.08 | 51.09 | 19.51 | 0.94 | 3.54 | 12.01 | 2.22 | 11.47 |

*Note.* Average grain size is qualitatively deduced from the image. Porosity and elements content are qualitatively obtained using ***ImageJ*** processing software, by applying thresholds on the different mineralogy images. From the content in silicium, assuming that no amorphous silica are present, the quartz (i.e., $SiO_2$) content is directly inferred. Combining contents in aluminum (Al) and potassium (K) or sodium (Na) elements, content in feldspars minerals can be inferred.

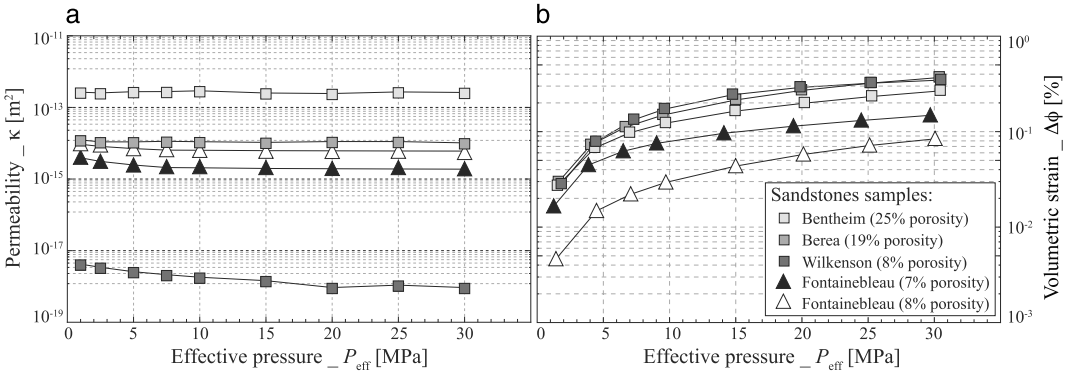


**Figure 3.** Measured physical properties of the sandstones investigated: (a) Permeability of the water-saturated rocks as a function of confining pressure. (b) Volumetric strain of the dry samples from the static ramps of confining pressure. The measurement from Pimienta, Fortin, and Guéguen (2015b) on a 7% and 8% porosity Fontainebleau sandstone samples is reported for comparison.

Comparing the volumetric strain variations (Figure 3b), all samples exhibit a transition from nonlinear variations at low $P_{eff}$ up to linear variations at higher $P_{eff}$. However, the characteristic pressure for the change of slope and the magnitude of variations differ from one rock to the other. Bentheim, Berea, and Wilkenson sandstones have very similar magnitudes of variations over the pressure range. Those variations have larger magnitudes than the ones of the Fontainebleau samples. It directly implies smaller stiffnesses (i.e., elastic moduli) than those of the Fontainebleau samples. In case of Wilkenson sandstone, as highlighted by the slope at higher pressures, the static bulk modulus reaches 30 GPa at $P_{eff} = 30$ MPa.

### 3.1.2. Elastic Dispersion at 1 MPa Effective Pressure

Owing to the range in permeability observed for the different sandstone samples, a specific fluid is chosen to saturate each of the rock samples. The reason is that the critical frequency for the drained/undrained transition (i.e., Biot-Gardner flow) varies as $\kappa/\eta$ (e.g., Cleary, 1978). To account for the viscosity effect (e.g., Batzle et al., 2006; Spencer & Shine, 2016), we define an apparent frequency $f^* = f(\eta/\eta_0)$, with $\eta_0 = 10^{-3}$ Pa s (e.g., Pimienta, Fortin, & Guéguen, 2015a). The properties of the high permeability Bentheim sandstone are investigated under glycerine saturation (i.e., high viscosity fluid). The properties of the lower permeability Berea sandstone are investigated under saturation of both glycerine and a water-glycerine mixture. The properties of the low permeability Wilkenson sandstone are investigated under water saturation (i.e., low viscosity) only. The samples properties are reported as a function of apparent frequency at lowest Terzaghi effective pressure of $P_{eff} = 1$ MPa (Figure 4). The elastic properties measured are (i) Young's modulus $E$, (ii) Poisson's ratio $\nu$, (iii) Young's modulus dissipation $Q_E^{-1}$, and (iv) Poisson's ratio dissipation $Q_\nu^{-1}$. The hydraulic property, addressed here as "fluid flow parameter," refers to the frequency-dependent pseudo-consolidation parameter (e.g., Pimienta, Fortin, Borgomano, et al., 2016), an in situ proxy of fluid flow out of the sample.

For all sandstone samples, both Young's modulus and Poisson's ratio show an increase with increasing apparent frequency. Yet different trends are observed for Young's modulus and Poisson's ratio. Young's modulus of Wilkenson sandstone slightly increases but remains in the range of [16,18] GPa for frequencies below $f^* = 10$ Hz (Figure 4b). Beyond this frequency, a steep increase is observed, up to about $E = 27$ GPa at 100 Hz. In case of Berea sandstone, a slow increase from $E = 20$ GPa to $E = 30$ GPa is observed over the frequency range of measurement (i.e., $f^* = [1; 3.10^4]$ Hz). For this rock, measurements under glycerine saturation are slightly shifted up as compared to the water-glycerine saturation. Young's modulus of Bentheim sandstone shows the largest increase, from $E = 31$ GPa up to $E = 52$ GPa. Similar to Wilkenson sandstone, a slow increase is observed at frequencies below $f^* = 2 - 5$ kHz. Beyond this frequency, a steep increase is observed.

For all rocks, Poisson's ratio increases with the measuring frequency (Figure 4b). The largest variation is observed for Wilkenson sandstone, that is, from $\nu = 0.24$ up to $\nu = 0.37$ as frequency increases. Beyond $f^*$=10 Hz, a plateau is reached and Poisson's ratio remains constant. Berea sandstone Poisson's ratio also shows a large increase, from $\nu = 0.25$ up to $\nu = 0.34$, at frequencies below $f^* = 1$ kHz. The values remain relatively constant in the range of $f^* = [1; 10]$ kHz and then decrease slightly beyond $f^*$=20 kHz. For Bentheim sandstone, an increase up to $\nu = 0.35$ is observed at $f^* = 10$ kHz. Beyond this frequency, $\nu$ remains constant.

Overall, the variations in $E$ and $\nu$ correlate with the measured dissipations (Figures 4c and 4d). The $Q_\nu^{-1}$ peaks are consistent with the monotonous variations in $\nu$. For Wilkenson and Bentheim sandstones, large increases

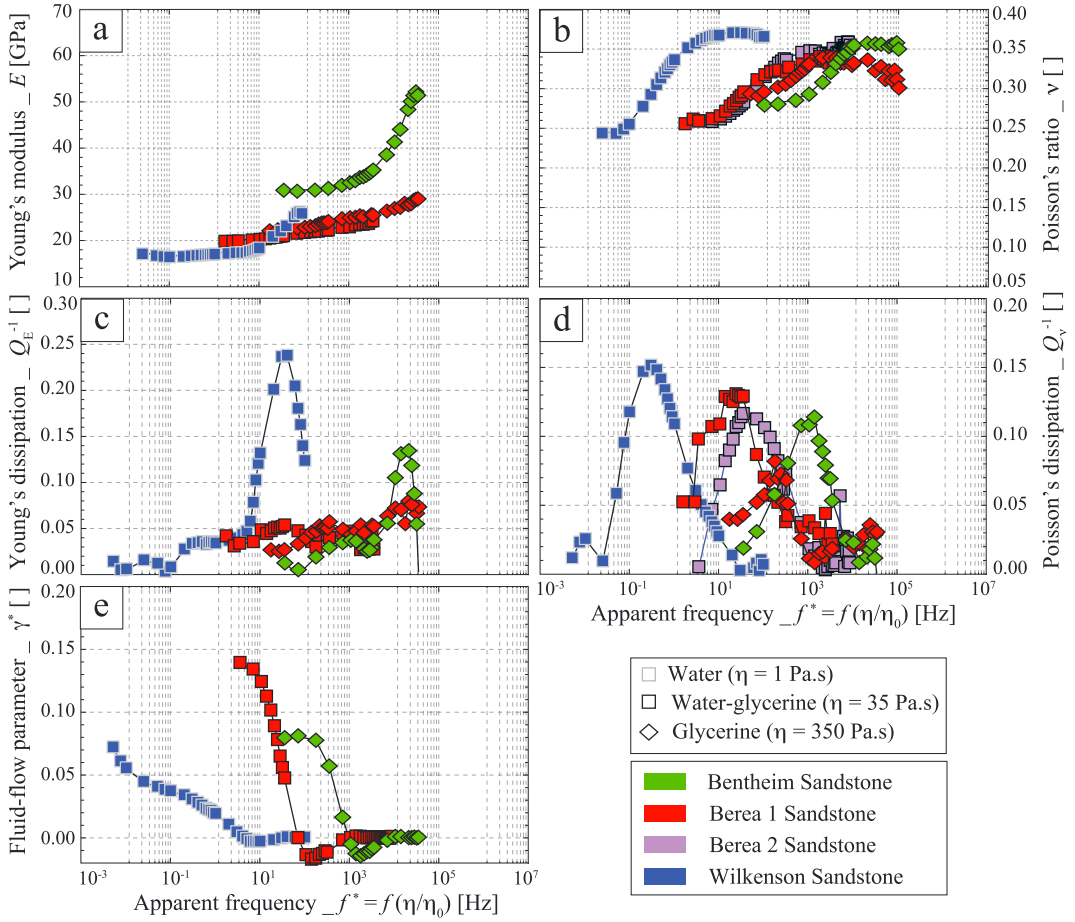


**Figure 4.** Measured (a) Young's modulus, (b) Poisson's ratio, (c-d) their related dissipations, and (e) the fluid-flow parameter as a function of apparent frequency in the fluid-saturated samples for an effective pressure of $P_{eff}$ = 1 MPa. The samples studied are a water-saturated Wilkenson sandstone, a glycerine-saturated Bentheim sandstone, and a Berea sandstone under either glycerine or water-glycerine saturation. The Poisson's ratio of the Berea sandstone is measured twice under water-glycerine saturation. The in situ liquid viscosity ($\eta$) used to determine the apparent frequency ($f^*$) is obtained from the measured hydraulic diffusivity for the different samples.

in $E$ and $\nu$ correlate with large peaks in $Q_E^{-1}$ and $Q_\nu^{-1}$. Consistently also, the almost linear increase in Berea sandstone Young's modulus correlates to a constant $Q_E^{-1} \sim 0.05$ over the frequency range. From the sample hydraulic response, a large frequency-dependent decrease in fluid flow is observed for all samples (Figure 4e). This indicates that, for $f^*$ beyond 10 Hz, 100 Hz, and 1 kHz, respectively, the Wilkenson, Berea, and Bentheim sandstones are undrained.

### 3.2. Role of Effective Confining Pressure

Different frequency dependences of Young's modulus and Poisson's ratio are observed for the different sandstones. For Bentheim and Wilkenson sandstones, $E$ and $Q_E^{-1}$ data are consistent with two distinct transitions in frequency. But this is not the case for $\nu$ and $Q_\nu^{-1}$ for which only one transition seems to exist. Moreover, large variations in $E$ and $\nu$ are observed over the frequency range. In the following, the pressure effect on these transitions is examined for the two rocks.

#### 3.2.1. Bentheim Sandstone

Elastic and hydraulic properties of the Bentheim sandstone sample under glycerine saturation are measured as a function of frequency for different effective pressures in the range of $P_{eff}$ = [1; 10] MPa (Figure 5). For all values of $P_{eff}$, an increase in $E$ (Figure 5a) and $\nu$ (Figure 5b) is observed with increasing frequency. This increase in elastic properties correlates to $Q_E^{-1}$ (Figure 5c) and $Q_\nu^{-1}$ (Figure 5d) peaks. Two peaks are observed on $Q_E^{-1}$ at $f_1$ = 3 Hz and $f_2$ = 50 Hz and one for $Q_\nu^{-1}$ at $f_1$ = 3 Hz. For all pressures, consistently with $E$, the first peak is

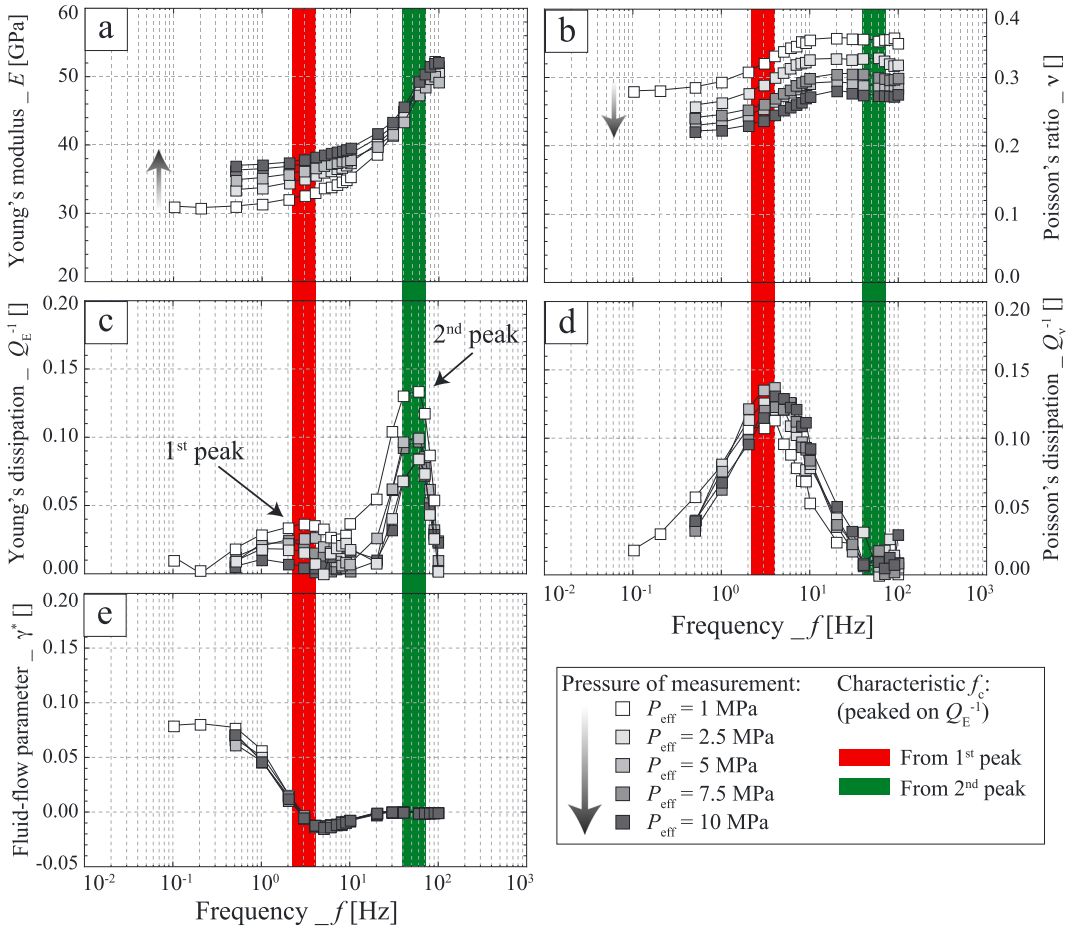


**Figure 5.** Measured frequency dependence of all available properties on a glycerine-saturated Bentheim sandstone for varying effective pressures in the range of [1;10] MPa. The properties measured are (a) Young's modulus, (b) Poisson's ratio, (c) Young's modulus associated dissipation (i.e., addressed as Young's attenuation), (d) Poisson's ratio associated dissipation (i.e., addressed as Poisson's attenuation), and (e) pseudo-consolidation parameter $\gamma^*$, direct indication of fluid flow out of the sample.

of much lower magnitude than the second, and the characteristic frequencies remain the same. By reporting the characteristic frequencies for the two $Q_E^{-1}$ peaks in all graphs, one notes that the $Q_\nu^{-1}$ peak occurs at $f_1$.

The fluid flow parameter (Figure 5e) shows a large frequency-dependent decrease, down to 0 beyond 10 Hz. Consistently, this value of 10 Hz corresponds to the frequency at which a change of slope is observed on $E$, and a plateau is reached for $\nu$. Interestingly, no effect of pressure on the fluid flow is observed. In terms of pressure dependence, $E$ and $\nu$ differ. Beyond 10 Hz, the dependence of $E$ to effective pressure is very small. A large dependence of $\nu$ to $P_{eff}$ is observed over the whole frequency range.

### 3.2.2. Wilkenson Sandstone

Wilkenson sandstone properties are measured as a function of frequency for pressures in the range of $P_{eff}$ = [1; 20] MPa (Figure 6). For all $P_{eff}$, two $Q_E^{-1}$ peaks and one $Q_\nu^{-1}$ peak are again observed, which correlates with the variations in $E$ and $\nu$. Similar to variations for the Bentheim sandstone, the first $Q_E^{-1}$ peak (at $f_1$ = 0.2 Hz) is much smaller than the second one (at $f_2$ = 40 Hz). The $Q_\nu^{-1}$ peak occurs again at the frequency $f_1$, and no variation is observed at $f_2$.

As for Bentheim sandstone, $P_{eff}$ affects differently the frequency dependence of $E$ (Figure 6a) and $\nu$ (Figure 6b). Consistently with the first $Q_E^{-1}$ peak, $E$ is shifted to higher values as $P_{eff}$ increases, so that dispersion decreases, yet the frequency dependence remains apparently unaffected by pressure. The second peak (i.e., at $f_2$) decreases down to half its initial value as $P_{eff}$ increases. Poisson's ratio decreases with $P_{eff}$, but the magnitude of dispersion (Figure 6b) and attenuation (Figure 6d) remains constant. Consistently, the amount of fluid flow decreases as $P_{eff}$ increases.

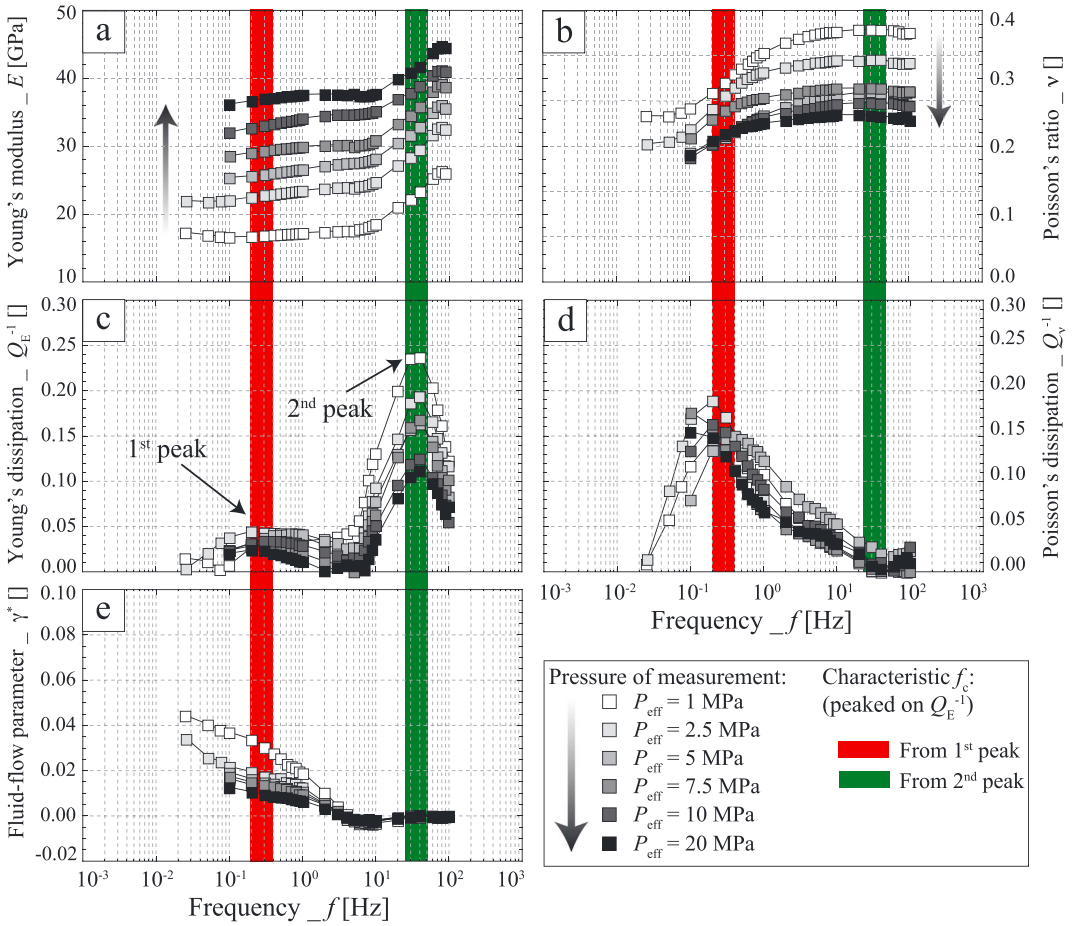


**Figure 6.** Measured frequency dependence of all available properties on a water-saturated Wilkenson sandstone for varying effective pressures in the range of [1;10] MPa. The properties measured are (a) Young's modulus, (b) Poisson's ratio, (c) Young's modulus associated dissipation (i.e., addressed as Young's attenuation), (d) Poisson's ratio associated dissipation (i.e., addressed as Poisson's attenuation), and (e) pseudo-consolidation parameter $\gamma^*$, direct indication of fluid flow out of the sample.

## 4. Interpretation : Dispersion/Attenuation in Sandstones Over the Frequency Range

Different effects are observed in the three different sandstones. In the following, to better investigate those variations, measurements are first compared to previous results on two Fontainebleau sandstones (Pimienta, Fortin, & Guéguen, 2015b, 2016) to attain a larger overview of frequency effects in sandstones. While different authors reported results on sandstones (e.g., Spencer & Shine, 2016), because the role of the measuring method was shown to be of major importance (e.g., Pimienta, Borgomano, et al., 2016), only measurements using the same apparatus and procedure are used in this part. A comparison between the different measurements methods is then discussed.

### 4.1. Variability of Frequency Effects in Sandstones: Microstructural Control

#### 4.1.1. Measured Frequency Effects in Five Sandstones

The frequency-dependent elastic properties of up to five sandstones samples can be compared over the frequency range (Figure 7). Note that two different porosities are investigated: (i) the two Fontainebleau and the Wilkenson sandstones have similar porosities in the range of $\phi = [7;9]$ % and (ii) the Bentheim and Berea sandstones have a similar porosity of $\phi = [20;25]$ %. Overall, a large variability can be observed between the five different sandstones. Very different characteristic frequencies are observed (Figure 7). Table 2 reviews the samples properties as well as the observed frequency of the variations for the different sandstone samples. The variability between the characteristic frequencies observed does not directly correlate to the sample porosity or mineral content.

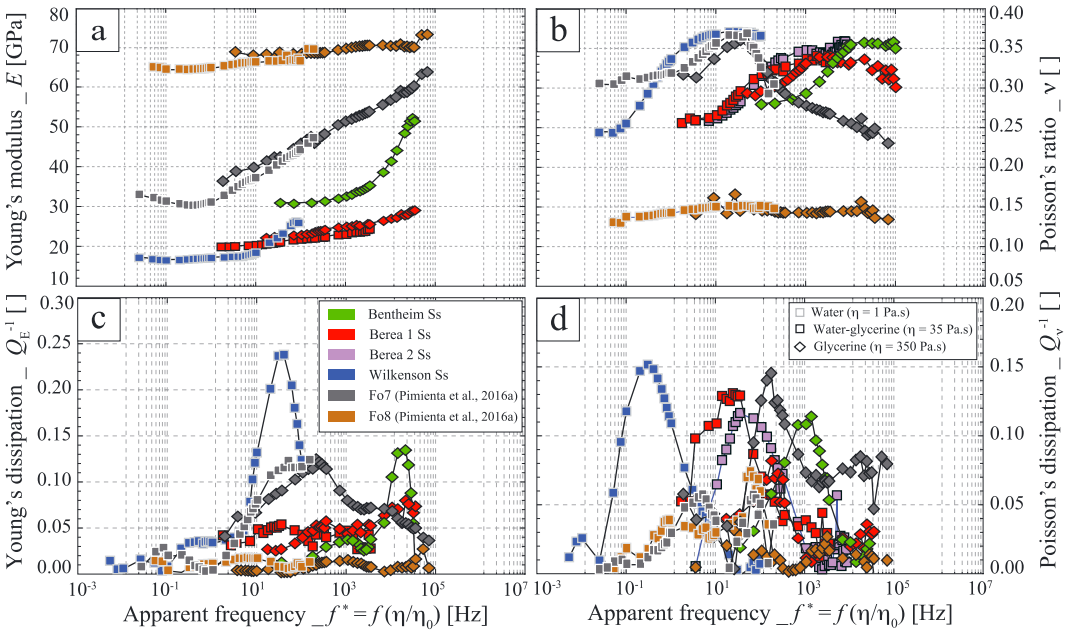


**Figure 7.** Comparison of the (a, b) Young's modulus $E$ and $Q_E^{-1}$ and (c, d) Poisson's ratio $\nu$ and $Q_\nu^{-1}$ as a function of apparent frequency for the five sandstone samples saturated by water (i.e., gray squares), glycerine (i.e., diamonds), and a water-glycerine mixture (i.e., black squares). In addition to the three sandstones studied, the Fontainebleau sandstone samples from Pimienta, Fortin, and Guéguen (2015b); Pimienta, Fortin, and Guéguen (2016) are reported for comparison.

In the available frequency range, two distinct fluid flow phenomena are expected to occur (e.g., Pimienta, Fortin, Borgomano, et al., 2016): (i) Biot-Gardner flow (i.e., drained/undrained transition), separating the drained and the undrained regimes, and (ii) squirt flow (i.e., undrained/unrelaxed transition), separating the undrained and the unrelaxed regimes. Both Fontainebleau sandstone samples (Pimienta, Fortin, & Guéguen, 2015b, 2016) were shown to exhibit both the Biot-Gardner (i.e., drained/undrained) and squirt flow (i.e., undrained/unrelaxed) transitions, leading to dispersion/attenuation on both Young's modulus and Poisson's ratio. But although of similar porosity (i.e., about 7% and 8%), the two samples showed evidence of very different behaviors. For the 7% porosity Fontainebleau sample, two large dispersion/attenuation effects were measured on both Young's modulus and Poisson's ratio. For the 8% porosity Fontainebleau sample, both critical frequencies overlapped, leading to a single transition from the drained to the unrelaxed regime.

For the three sandstones examined in this work, a dispersion/attenuation effect is observed on both Young's modulus and Poisson's ratio in the low-frequency range. At higher frequency, very different behaviors are observed for the three rocks. From the slope change in $E$ and $\nu$ at highest frequency, the beginning of a second frequency-dependent dispersion/attenuation phenomena is observed for Berea sandstone. For Wilkenson

**Table 2**
*Properties Measured for the Five Rock Samples at an Effective Pressure of $P_{eff} \sim 1$ MPa*

| Sample # | Fo7 | Fo8 | WilkS | BeS | BhS |
|---|---|---|---|---|---|
| Porosity ($\phi$) | 7.2% | 8.7% | 9.1% | 19.2% | 24.8% |
| Quartz content | 99.9% | 99.9% | 51.1% | 81.7% | 97.9% |
| Permeability ($\kappa$ in m$^2$) | $4 \times 10^{-15}$ | $1 \times 10^{-14}$ | $3 \times 10^{-18}$ | $2 \times 10^{-14}$ | $5 \times 10^{-13}$ |
| Drained bulk modulus ($K_d$) | 7 GPa | 25 GPa | 7 GPa | 5 GPa | 5 GPa |
| Frequency ($f^*_{obs1}$) | 10 Hz | 20 Hz | 0.3 Hz | 30–300 Hz | 1 kHz |
| Frequency ($f^*_{obs2}$) | 1 kHz | – | 30 Hz | 20–40 kHz | 10 kHz |

*Note.* Porosity and quartz content are from SEM-EDS images. Permeability and bulk modulus are measured at $P_{eff} \sim 1$ MPa. Frequency is picked from the $Q_E^{-1}$ peaks. Results on the Fontainebleau are from Pimienta, Fortin, and Guéguen (2015a); Pimienta, Fortin, and Guéguen (2016).

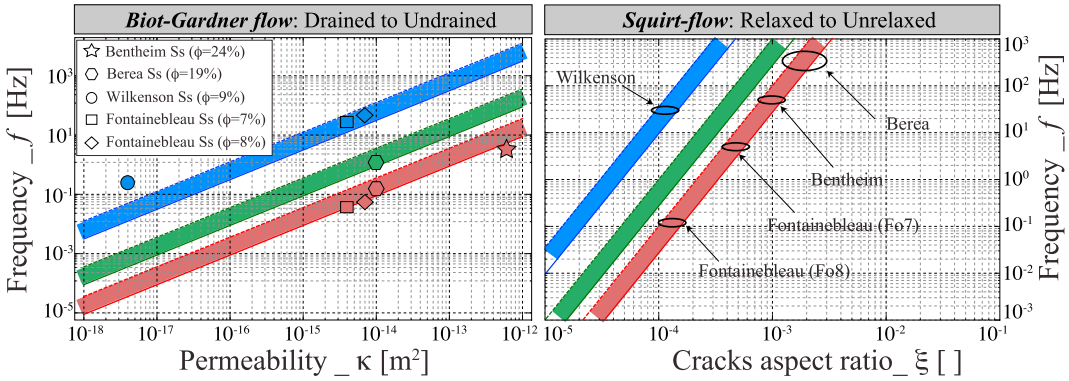


**Figure 8.** Comparison plot of the predicted characteristic frequency for the (a) Biot-Gardner flow and (b) squirt flow phenomena. The frequency is calculated from equations (1) and (2) using three different fluid viscosities (i.e., blue for water, green for the water-glycerine mixture, and red for glycerine). For the two transitions, domains of realistic of frequency values are drawn by using a range of realistic parameters (i.e., $K_d = [5, 15]$ GPa, $L = [40, 80]$ mm, and $K_s = [35, 40]$ GPa).

and Bentheim sandstones, a second frequency effect is clearly observed. For both rocks, only Young's modulus and its dissipation seem to be affected by the second effect.

#### 4.1.2. Fluid Flow Theories: Apparent Frequency Versus Microstructure

According to Cleary (1978) and O'Connell and Budiansky (1977), the two transitions relate to a characteristic frequency that depends on microstructural variables of the rock sample. The Biot-Gardner flow (i.e., drained/undrained transition) separates the drained regime (i.e., flow out of a volume) and the undrained regime (i.e., fluid pressurization in the volume). As shown by Cleary (1978), this transition is proportional to the rock hydraulic conductivity (i.e., $\kappa/\eta$) and a fluid diffusion length $L$ such that

$$f_1 = \frac{4\kappa K_d}{\eta L^2}, \tag{1}$$

where $\eta$ is the fluid viscosity and $K_d$ and $\kappa$ are, respectively, the drained bulk modulus and the permeability of the investigated rock sample. In the experimental conditions, $L$ is a length associated to the rock sample size (e.g., Adelinet et al., 2011). $L$ is expected to be between the sample length and half of it, that is, $L \in [40; 80]$ mm. At higher frequencies, fluid has no more time to equilibrate in the REV (representative elementary volume) so that a third flow regime is present that is called "unrelaxed." Since, in general, a porous rock contains inclusions of different shapes (i.e., pores and microcracks), fluid can flow from a compliant microcrack to a neighboring less compliant pore (O'Connell & Budiansky, 1977). This squirt flow phenomenon is associated with a critical frequency that depends on the skeleton bulk modulus (i.e., $K_s$), on the microcrack aspect ratio $\xi$ and on the fluid viscosity $\eta$ such that (O'Connell & Budiansky, 1977)

$$f_2 = \frac{\xi^3 K_s}{\eta}. \tag{2}$$

Using realistic parameters (i.e., $K_d \in [5; 15]$ GPa, $L \in [40; 80]$ mm, $K_s \in [35, 40]$ GPa), range of values can be predicted for $f_1$ (equation (1) and $f_2$ (equation (2). Figure (8) compares the observed characteristic frequencies $f$ for the different attenuation peaks to the predicted ranges for $f_1$ and $f_2$. In case of Biot-Gardner flow, the theory predicts an increase in the cutoff frequency as permeability increases or as fluid viscosity decreases. The two parameters being measured directly and with accuracy, it is possible to compare directly measurements and prediction (Figure 8a). Overall, a good fit is observed for all rock samples and all saturating fluids. In case of squirt flow (Figure 8b), the characteristic frequency is controlled by the aspect ratio of microcracks, a parameter not measurable directly with accuracy in rocks. Comparing the predicted and observed critical frequency, a range of aspect ratio is assessed for all rock samples: About $\xi = 10^{-4}$ in both the Wilkenson sandstone and in Fo8, a slightly higher value of about $\xi = 5\,10^{-4}$ for Fo7, and larger values of $\xi = 1 - 3\,10^{-3}$ for Bentheim and Berea sandstones. These aspect ratio values are realistic for sandstones (e.g., David et al., 2013; Fortin et al., 2007, 2014; Walsh, 1965) and could be inferred from different methods (e.g., De Paula et al., 2012). Ultimately comparing the results of Figure 8 with the ones of Table 2, different dependences to the permeability, porosity, and mineral content are observed: (i) Consistent with equation (1), the first transition correlates

to permeability, which in turn is dependent on porosity and mineral content. For similar porosities, permeability decreases as the content in clay mineral increases and (ii) as expected from equation (2), the frequency for the second transition is independent of the rock permeability.

Note finally that the first transition correlates with a fluid flow out of the sample (Figure 4e). Consistent with results on the two Fontainebleau sandstones (Pimienta, Fortin, & Guéguen, 2016), the much larger dispersion/attenuation in Poisson's ratio than Young's modulus for this transition is expected. Following Biot-Gassmann theory, the rock shear modulus $G$ is expected to be constant for this transition. From linear elasticity in an isotropic medium

$$E = 2G(1 + \nu). \tag{3}$$

Assuming linear viscoelasticity, one gets

$$\frac{\Delta E}{E} = \frac{\Delta \nu}{\nu} \frac{\nu}{(1 + \nu)} \approx 0.3 \frac{\Delta \nu}{\nu}. \tag{4}$$

Hence, the small effect on Young's modulus is consistent. These additional information confirm that the first dispersion/attenuation phenomenon is caused by the transition from drained to undrained regime.

### 4.2. Zener Rheological Model : Fluid Flow in the High-Frequency Range

Large dispersion/attenuation on Young's modulus are observed at high frequencies in Bentheim and Wilkenson sandstones, when no flow out of the sample occurs anymore. Are the observed variations in modulus and dissipation consistent with a linear viscoelastic behavior? Indeed, viscoelasticity is a robust way to test the measured variations in modulus and the measured dissipation (e.g., Borgomano et al., 2017; Mikhaltsevitch et al., 2016b; Pimienta, Fortin, & Guéguen, 2015a). Kramers-Kronig equations, expressing the causality principle between dispersion and dissipation, could be used (e.g., Mikhaltsevitch et al., 2016b). A simpler approach is to use Zener rheological model (e.g., Borgomano et al., 2017), which follows Kramers-Kronig principle but assumes only a single relaxation time. This assumption may not be valid if, for instance, there is a broad spectrum of crack aspect ratio. Consistent with what has been already described in other works (e.g., Borgomano et al., 2017; Pimienta, Fortin, & Guéguen, 2015a, 2015b), the first transition can be shown to follow Kramers-Kronig causality principle for all samples. This is expected as quasi-static poroelasticity fits the viscoelastic framework (e.g., Rubino et al., 2008). This should theoretically be the case also for the squirt flow effect (e.g., Carcione & Gurevich, 2011; De Paula et al., 2012). It is thus of interest to investigate the links between measurements and viscoelasticity for this second transition.

For the two Fontainebleau sandstones, it was also shown to be true but one sample did not follow the Zener-like frequency dependence (e.g., Pimienta, Fortin, & Guéguen, 2015b). For Wilkenson sandstone (Figures 9b and 9d), an excellent fit is observed between data and Zener model predictions. Because both the amplitude and the bandwidth of the peak fit, it further implies that only one relaxation time, that is, only one single family of aspect ratio, is observed in this frequency range. Combining with the results of Figure 8b, the cracks family has an inferred average aspect ratio of $\xi = 10^{-4}$. For Bentheim sandstone, however, the $E$ variations and the $Q_E^{-1}$ peak do not fit (Figures 9a and 9c). Fitting Zener model to the $E$ variations, the predicted attenuation peak is of 0.20, higher than the data that indicate a maximum of $Q_E^{-1} = 0.15$. Moreover, the peak bandwidth is not consistent with a Zener-like model. Such effect could be due to either (i) a lower accuracy on $Q_E^{-1}$ or (ii) the existence of phenomenon that deviates from viscoelasticity. A possible low accuracy in the measurement of $Q_E^{-1}$ is likely and cannot be ruled out at this point. However, could another physical effect be the cause of an uncoupling between dispersion and attenuation? Interestingly, out of the sandstones studied, Bentheim sandstone is the most porous (i.e., $\phi = 24\%$) and permeable (i.e., $\kappa = 5 \times 10^{-13}$ m$^2$).

## 5. Discussion: Other Data Sets and Effect of the Measuring Method

In section 4, no comparison was made with other data sets as very different experimental methods have been used by other authors. However, it is important to compare the results to other published data in order to gain a better insight on the effects, independently of the measuring setup and conditions.

### 5.1. Previous Measurements on Berea Sandstone

In comparison with other sandstones (e.g., Fontainebleau sandstone) showing large variabilities, elastic properties for different Berea sandstone samples are similar (e.g., Pimienta et al., 2014). In the framework of the

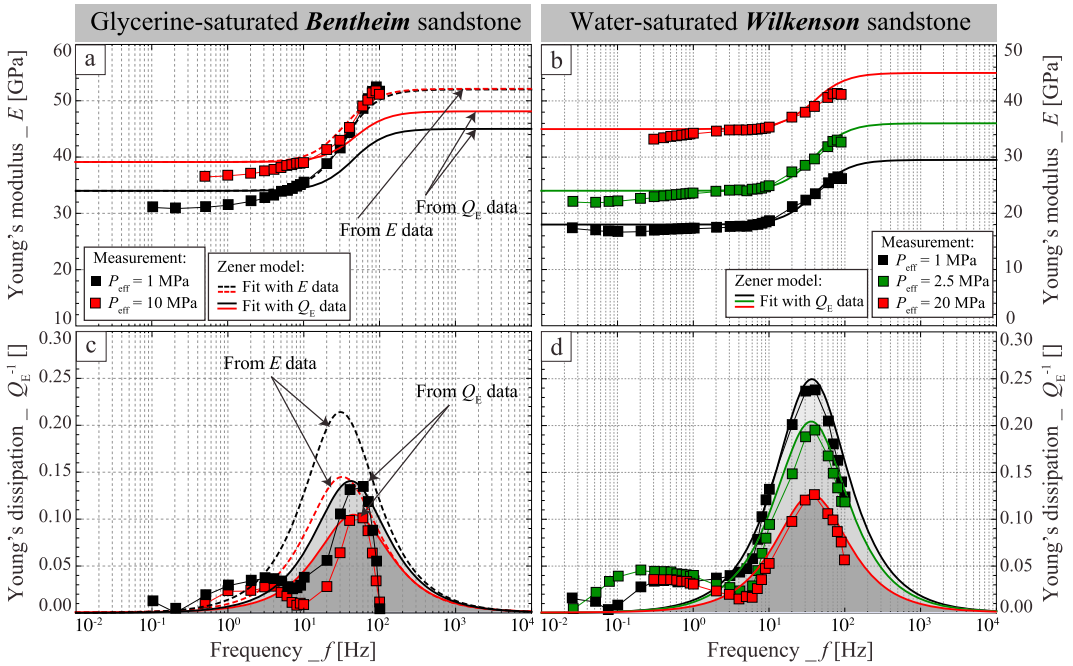


**Figure 9.** Comparison between measured (a, b) Young's modulus $E$ and its related (c, d) Young's dissipation for the second frequency-dependent variation using Zener rheological models. Only the magnitude of the effect is of interest here, and the dashpot viscosity is adjusted to fit the frequency dependence. For the glycerine-saturated Bentheim sandstone, two comparisons are tested, from using either the data of $E$ (i.e., dashed lines) or of $Q_E^{-1}$ (i.e., continuous lines).

investigation of the frequency dependence of elastic properties, samples of this rock were measured by Tisato and Madonna (2012), Chapman et al. (2016), Mikhaltsevitch et al. (2016a), Spencer and Shine (2016), and in this study. Tisato and Madonna (2012) and Chapman et al. (2016) investigated mainly effects under partial saturation conditions. As in this work, Mikhaltsevitch et al. (2016a) and Spencer and Shine (2016) measured a Berea sandstone under full saturation by fluids of varying viscosity. As shown in Table 3, porosity is relatively similar for all samples but variable permeabilities are observed in the samples. The sample used by Spencer and Shine (2016) has a permeability 2 orders of magnitudes larger than the one used in this study. The sample used by Mikhaltsevitch et al. (2016a) is similar to that of this study. Interestingly, one observes a good correlation between permeability and cutoff frequency observed by the authors: the effect for Spencer and Shine (2016) occurs at frequency $f^* = 40$ kHz that is 2 orders of magnitude higher than $f^* = 0.3–0.5$ kHz found in this study and in Mikhaltsevitch et al. (2016a). Moreover, comparing results on Young's modulus and Poisson's ratio by Mikhaltsevitch et al. (2016a) with the ones in this study, a very good fit is observed in both magnitude and frequency dependence of the effects.

**Table 3**
*Comparison of Measured Physical Properties (i.e., Porosity, Quartz Content, and Permeability) by Different Teams on Berea Sandstone: (1) This Study, (2) Mikhaltsevitch et al. (2016a), and (3) Spencer and Shine (2016)*

| Study # | (1) | (2) | (3) |
|---|---|---|---|
| Porosity ($\phi$) | 19.2% | 19% | 24.4% |
| Quartz content | 81.7% | 80% | – |
| Permeability ($\kappa$ in m$^2$) | $2 \times 10^{-14}$ | $7.1 \times 10^{-14}$ | $1.3 \times 10^{-12}$ |
| Drained bulk modulus ($K_d$) | 5 GPa | – | – |
| Frequency ($f^* = f(\eta/\eta_0)$) | 0.3 kHz | 0.5 kHz | 40 kHz |

*Note*. For the three studies, the sample is measured under glycerin full saturation. The reported frequency is the one corresponding to the $Q_E^{-1}$ peak in the different studies, by normalizing the fluid viscosity to obtain $f^*$.

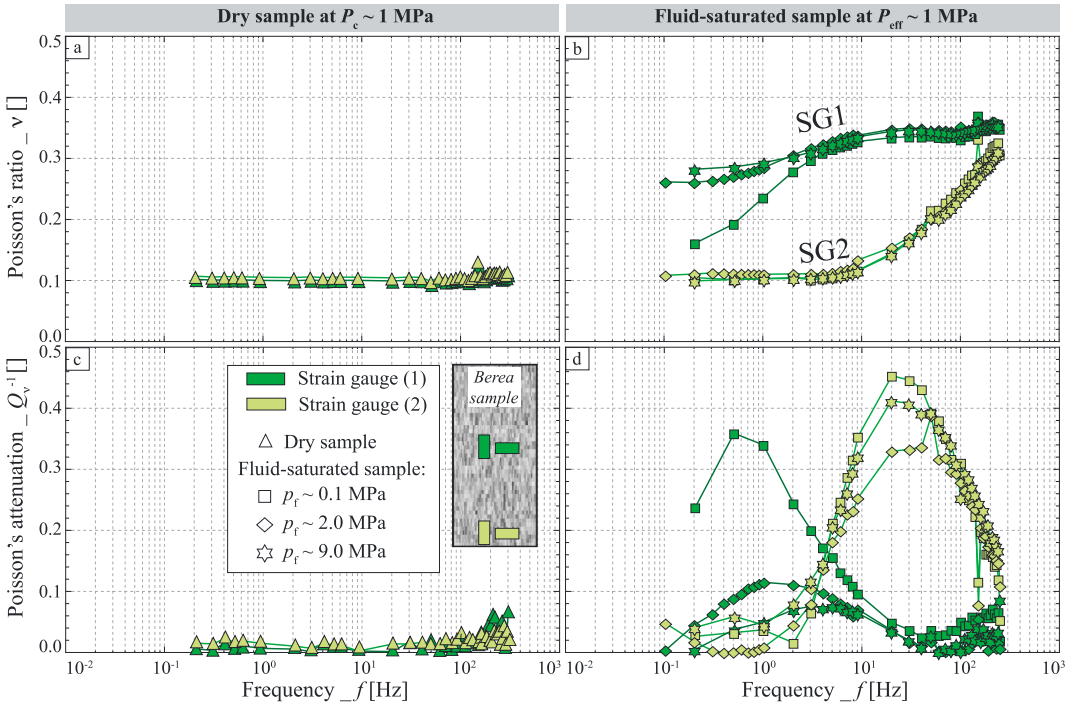


**Figure 10.** Measured frequency dependence of (a, b) Poisson's ratio and (c, d) its associated dissipation in a Berea sandstone sample at a Terzaghi effective pressure of $P_{eff} = 1$ MPa. The sample is either Figures 10a and 10c) dry or Figures 10b and 10d saturated by a water-glycerine mixture. Under both dry and liquid-saturated conditions, the role of the measuring position is tested from measuring the strains at sample's half-length (i.e., dark green) or near the sample's bottom (i.e., light green). Under liquid-saturated conditions, the role of pore fluid pressure is tested while keeping a Terzaghi effective pressure of $P_{eff} = 1$ MPa.

Mikhaltsevitch et al. (2016a) and Spencer and Shine (2016) interpreted the measured dispersion/attenuation as induced by squirt flow phenomena. The present paper reports also the hydraulic response that was not measured with other setups. This confirms in our case that the observed transition is the transition between drained and undrained elastic regimes. It is possible that they measured also the Biot-Gardner flow: a transition from partially drained (Pimienta, Borgomano, et al., 2016) to undrained regime. The same possibility holds for the data of Spencer and Shine (2016). It could be also that Spencer and Shine (2016) measured an effect that is a combination of the two transitions, similar to what was observed on the Fo8 sample by Pimienta, Fortin, and Guéguen (2015a).

### 5.2. Role of the Measuring Method Over the Frequency Range

Pimienta, Borgomano, et al. (2016) showed theoretically that "global" or "local" measurements, or local measurements in different localizations, would lead to different apparent behaviors of the rock sample. To investigate this effect, the second experiment on the Berea sample reported in Figures 4b and 4d was measured with a different setup. Strain gages were glued at different axial positions on the sample, that is, at the middle length (i.e., dark green symbols in Figure 10) and near the end platen (i.e., light green symbols in Figure 10). Moreover, the effect of changing the fluid pressure on the measurement was also tested. The dispersion/attenuation measurements on the sample under dry and fluid-saturated conditions are reported in Figure 10. Under dry conditions, consistently, no frequency dependence is observed, and no differentiation is made between the strain gages positions. Under saturation by the water-glycerine mixture, large deviations are observed depending on the strain gage positions.

For the strain gage positioned in the middle of the sample (i.e., dark green symbols), results are the same as those previously obtained (Figures 4b and 4d). At lowest frequency, because the rock is partially undrained (Pimienta, Fortin, & Guéguen, 2016), Poisson's ratio is much larger than under dry conditions (Figure 10b). At very low pore fluid pressure (i.e., $p_f = 0.1$ MPa), because it gets more difficult for fluid to pressurize in the dead volume and oppose the sample strain, values are initially much lower and then strongly increase with frequency to reach the same value in the undrained regime. For all $p_f$ values, the effect occurs in approximately

the same frequency range of $f \in [10^{-1}, 10^{1}]$ Hz. In case of the strain gauge located near the end platen (i.e., light green symbols), the values initially fit with the ones under dry conditions. Then, as frequency increases beyond $f = 10$ Hz, a dramatic increase is measured, leading to values close to the previous ones (Figure 10b). Interestingly, in this case, no effect of $p_f$ is observed. Note further that, in both cases, dispersion (Figures 10a and 10b) and attenuation (Figures 10c and 10d) fit with Zener models. The effects are also consistent with predictions from a simple 1D model to account for boundary effects on the measurements (Pimienta, Borgomano, et al., 2016).

Hence, the measuring position appears to lead to very different results. Spencer and Shine (2016) used capacitive displacement sensors, a setup measuring the global response of the sample, a response expected to average all local measurements across the sample length (Pimienta, Borgomano, et al., 2016). Then, the results should be in between the two responses in Figures 10b and 10d, with a transition spanning several orders of magnitude in frequency. Note that, consistently, Spencer and Shine (2016) data show dispersion/attenuation phenomena over more than 4 orders of magnitude in frequency. Mikhaltsevitch et al. (2016a) used a local method, as in our study, which is consistent with the very similar response in terms of frequency range and magnitude of the effect. Note finally that squirt flow phenomena are not expected to be dependent on the measured location, provided that the sample is homogeneous, that is, that each REV of the sample is the same.

## 6. Conclusion

Young's modulus and Poisson's ratio of different sandstones, saturated by different fluids, have been measured as a function of frequency. Large frequency-dependent variations are observed for all sandstones. The measured transitions differ in the characteristic frequency of occurrence, magnitude, or amount of elastic constants involved. Further comparing with published data, two different effects are observed for all samples over the allowed frequency range. Overall, the drained/undrained transition is observed for all samples. The characteristic frequency for this effect is consistent with the measured permeabilities. At higher frequency, a second effect is also observed that is, however, more difficult to assess. Interpreting this second transition in terms of squirt flow effect yields very realistic aspect ratio families for all rock samples. For the second effect, large dispersions and attenuation are measured for Wilkenson and Bentheim sandstones. In case of Bentheim sandstone, the measured dispersion and attenuation do not fit with Zener-like variations. This implies either that the measured dissipation is not accurate or that another physical effect is here observed. Noting that the sample is much more permeable than the others, its large pore entry diameters could be a cause for this effect. Ultimately, Berea sandstone is used as a comparison mean with published data by other teams. Very consistent results are observed. Experimental evidence of a strong control by the measuring method and conditions is highlighted in case of the drained to undrained transition. In case of squirt flow, no effect is expected.

**Acknowledgments**
This work has been supported by TOTAL, under project FR00007429. The first author wishes to thank Damien Deldicque for his help in using the SEM-EDS cartography setup, and the authors thank B. Quintal and B. Gurevich for their constructive reviews. The presented data sets are available upon request.

## References

Adelinet, M., Fortin, J., & Guéguen, Y. (2011). Dispersion of elastic moduli in a porous-cracked 431 rock: Theoretical predictions for squirt-flow. *Tectonophysics*, *503*(1), 173–181. https://doi.org/10.1016/j.tecto.2010.10.012

Adelinet, M., Fortin, J., Guéguen, Y., Schubnel, A., & Geoffroy, L. (2010). Frequency and fluid effects on elastic properties of basalt: Experimental investigations. *Geophysical Research Letters*, *37*, L02303. https://doi.org/10.1029/2009GL041660

Amalokwu, K., Papageorgiou, G., Chapman, M., & Best, A. I. (2017). Modelling ultrasonic laboratory measurements of the saturation dependence of elastic modulus: New insights and implications for wave propagation mechanisms. *International Journal of Greenhouse Gas Control*, *59*, 148–159.

Batzle, M., Hofmann, R., Han, D.-H., & Castagna, J. (2001). Fluids and frequency dependent seismic velocity of rocks. *The Leading Edge*, *20*(2), 168–171.

Batzle, M. L., Han, D.-H., & Hofmann, R. (2006). Fluid mobility and frequency-dependent seismic velocity—direct measurements. *Geophysics*, *71*(1), N1–N9.

Biot, M. A. (1941). General theory of three-dimensional consolidation. *Journal of Applied Physics*, *12*(2), 155–164.

Blöcher, G., Reinsch, T., Hassanzadegan, A., Milsch, H., & Zimmermann, G. (2014). Direct and indirect laboratory measurements of poroelastic properties of two consolidated sandstones. *International Journal of Rock Mechanics and Mining Sciences*, *67*, 191–201.

Borgomano, J. V. M., Pimienta, L., Fortin, J., & Guéguen, Y. (2017). Dispersion and attenuation measurements of the elastic moduli of a dual-porosity limestone. *Journal of Geophysical Research: Solid Earth*, *122*, 2690–2711. https://doi.org/10.1002/2016JB013816

Carcione, J., & Gurevich, B. (2011). Differential form and numerical implementation of BiotŠs poroelasticity equations with squirt dissipation. *Geophysics*, *76*, N55–N64.

Chapman, S., Tisato, N., Quintal, B., & Holliger, K. (2016). Seismic attenuation in partially saturated Berea sandstone submitted to a range of confining pressures. *Journal of Geophysical Research: Solid Earth*, *121*, 1664–1676. https://doi.org/10.1002/2015JB012575

Christensen, N. I., & Wang, H. F. (1985). The influence of pore pressure and confining pressure on dynamic elastic properties of Berea sandstone. *Geophysics*, *50*(2), 207–213.

Cleary, M. P. (1978). Elastic and dynamic response regimes of fluid-impregnated solids with diverse microstructures. *International Journal of Solids and Structures*, *14*(10), 795–819.

David, E. C., Fortin, J., Schubnel, A., Guéguen, Y., & Zimmerman, R. W. (2013). Laboratory measurements of low-and high-frequency elastic moduli in Fontainebleau sandstone. *Geophysics*, *78*(5), D369–D379.
De Paula, O. B., Pervukhina, M., Makarynska, D., & Gurevich, B. (2012). Modeling squirt dispersion and attenuation in fluid-saturated rocks using pressure dependency of dry ultrasonic velocities. *Geophysics*, *77*(3), WA157–WA168.
Duda, M., & Renner, J. (2013). The weakening effect of water on the brittle failure strength of sandstone. *Geophysical Journal International*, *192*(3), 1091–1108.
Dunn, K.-J. (1987). Sample boundary effect in acoustic attenuation of fluid-saturated porous cylinders. *The Journal of the Acoustical Society of America*, *81*, 1259–1266.
Fortin, J., Guéguen, Y., & Schubnel, A. (2007). Effects of pore collapse and grain crushing on ultrasonic velocities and $V_p/V_s$. *Journal of Geophysical Research*, *112*, B08207. https://doi.org/10.1029/2005JB004005
Fortin, J., Pimienta, L., Guéguen, Y., Schubnel, A., David, E. C., & Adelinet, M. (2014). Experimental results on the combined effects of frequency and pressure on the dispersion of elastic waves in porous rocks. *The Leading Edge*, *33*(6), 648–654.
Gardner, G. H. F. (1962). Extensional waves in fluid-saturated porous cylinders. *The Journal of the Acoustical Society of America*, *34*(1), 36–40.
Hart, D. J., & Wang, H. F. (2010). Variation of unjacketed pore compressibility using Gassmann's equation and an overdetermined set of volumetric poroelastic measurements. *Geophysics*, *75*(1), N9–N18.
Jackson, I., & Paterson, M. S. (1987). Shear modulus and internal friction of calcite rocks at seismic frequencies: Pressure, frequency and grain size dependence. *Physics of the Earth and Planetary Interiors*, *45*(4), 349–367.
Klein, E., Baud, P., Reuschlé, T., & Wong, T. F. (2001). Mechanical behaviour and failure mode of Bentheim sandstone under triaxial compression. *Physics and Chemistry of the Earth, Part A: Solid Earth and Geodesy*, *26*(1), 21–25.
Louis, L., David, C., Metz, V., Robion, P., Menendez, B., & Kissel, C. (2005). Microstructural control on the anisotropy of elastic and transport properties in undeformed sandstones. *International Journal of Rock Mechanics and Mining Sciences*, *42*(7), 911–923.
Madonna, C., & Tisato, N. (2013). A new seismic wave attenuation module to experimentally measure low-frequency attenuation in extensional mode. *Geophysical Prospecting*, *61*(2), 302–314.
Mavko, G., & Vanorio, T. (2010). The influence of pore fluids and frequency on apparent effective stress behavior of seismic velocities. *Geophysics*, *75*(1), N1–N7.
Mavko, G., Kjartansson, E., & Winkler, K. (1979). Seismic wave attenuation in rocks. *Reviews of Geophysics*, *17*(6), 1155–1164.
Mikhaltsevitch, V., Lebedev, M., & Gurevich, B. (2014). A laboratory study of low-frequency wave dispersion and attenuation in water-saturated sandstones. *The Leading Edge*, *33*(6), 616–622.
Mikhaltsevitch, V., Lebedev, M., & Gurevich, B. (2015). A laboratory study of attenuation and dispersion effects in glycerol-saturated Berea sandstone at seismic frequencies. In *Proceedings of seg 85th annual meeting, Society of Exploration Geophysicists* (pp. 3085–3089).
Mikhaltsevitch, V., Lebedev, M., & Gurevich, B. (2016a). An experimental evidence of the squirt-flow effect in glycerol-saturated Berea sandstone at seismic frequencies. In *Proceedings of the 78th Eage Conference and exhibition* (pp. 3085–3089).
Mikhaltsevitch, V., Lebedev, M., & Gurevich, B. (2016b). Validation of the laboratory measurements at seismic frequencies using the kramers-kronig relationship. *Geophysical Research Letters*, *43*, 4986–4991. https://doi.org/10.1002/2016GL069269
Müller, T. M., Gurevich, B., & Lebedev, M. (2010). Seismic wave attenuation and dispersion resulting from wave-induced flow in porous rocks: A review. *Geophysics*, *75*(5), 75A147–75A164.
O'Connell, R. J., & Budiansky, B. (1977). Viscoelastic properties of fluid-saturated cracked solids. *Journal of Geophysical Research*, *82*(36), 5719–5735.
Pagoulatos, A., & Sondergeld, C. (2004). Evaluation of multistage triaxial testing on Berea sandstone (Master's Thesis), University of Oklahoma, Norman, Oklahoma.
Papageorgiou, G., Amalokwu, K., & Chapman, M. (2016). Theoretical derivation of a Brie-like fluid mixing law. *Geophysical Prospecting*, *64*(4), 1048–1053.
Pimienta, L., Sarout, J., Esteban, L., & Delle Piane, C. (2014). Prediction of rocks thermal conductivity from elastic wave velocities, mineralogy and microstructure. *Geophysical Journal International*, *197*(2), 860–874.
Pimienta, L., Fortin, J., & Guéguen, Y. (2015a). Bulk modulus dispersion and attenuation in sandstones. *Geophysics*, *80*(2), D111–D127.
Pimienta, L., Fortin, J., & Guéguen, Y. (2015b). Experimental study of YoungŠs modulus dispersion and attenuation in fully saturated sandstones. *Geophysics*, *80*(5), L57–L72.
Pimienta, L., Borgomano, J. V. M., Fortin, J., & Guéguen, Y. (2016). Modelling the drained/undrained transition: Effect of the measuring method and the boundary conditions. *Geophysical Prospecting*, *64*(4), 1098–1111.
Pimienta, L., Fortin, J., & Guéguen, Y. (2016). Effect of fluids and frequencies on PoissonŠs ratio of sandstone samples. *Geophysics*, *81*(2), D183–D195.
Pimienta, L., Fortin, J., Borgomano, J. V., & Guéguen, Y. (2016). Dispersions and attenuations in a fully saturated sandstone: Experimental evidence for fluid flows at different scales. *The Leading Edge*, *35*(6), 495–501.
Pimienta, L., Fortin, J., & Guéguen, Y. (2017). New method for measuring compressibility and poroelasticity coefficients in porous and permeable rocks. *Journal of Geophysical Research: Solid Earth*, *122*, 2670–2689. https://doi.org/10.1002/2016JB013791
Prasad, M., & Manghnani, M. H. (1997). Effects of pore and differential pressure on compressional wave velocity and quality factor in Berea and Michigan sandstones. *Geophysics*, *62*(4), 1163.
Riviere, J., Pimienta, L., Scuderi, M., Candela, T., Shokouhi, P., Fortin, J., … Johnson, P. A. (2016). Frequency, pressure, and strain dependence of nonlinear elasticity in Berea sandstone. *Geophysical Research Letters*, *43*, 3226–3236. https://doi.org/10.1002/2016GL068061
Rubino, J. G., Ravazzoli, C. L., & Santos, J. E. (2008). Equivalent viscoelastic solids for heterogeneous fluid-saturated porous rocks. *Geophysics*, *74*(1), N1–N13.
Sarout, J. (2012). Impact of pore space topology on permeability, cut-off frequencies and validity of wave propagation theories. *Geophysical Journal International*, *189*, 481–492.
Sayers, C. M., Van Munster, J. G., & King, M. S. (1990). Stress-induced ultrasonic anisotrophy in Berea sandstone. In *International Journal of Rock Mechanics and Mining Sciences & Geomechanics Abstracts* (Vol. 27, pp. 429–436). Elsevier.
Spencer, J. W. (1981). Stress relaxations at low frequencies in fluid-saturated rocks: Attenuation and modulus dispersion. *Journal of Geophysical Research*, *86*(B3), 1803–1812.
Spencer, J. W., & Shine, J. (2016). Seismic wave attenuation and modulus dispersion in sandstones. *Geophysics*, *81*(3), D211–D231.
Subramaniyan, S., Quintal, B., Madonna, C., & Saenger, E. H. (2015). Laboratory-based seismic attenuation in Fontainebleau sandstone: Evidence of squirt flow. *Journal of Geophysical Research: Solid Earth*, *120*, 7526–7535. https://doi.org/10.1002/2015JB012290
Subramaniyan, S., Quintal, B., Tisato, N., Saenger, E. H., & Madonna, C. (2014). An overview of laboratory apparatuses to measure seismic attenuation in reservoir rocks. *Geophysical Prospecting*, *62*(6), 1211–1223.

Szewczyk, D., Bauer, A., & Holt, R. M. (2016). A new laboratory apparatus for the measurement of seismic dispersion under deviatoric stress conditions. *Geophysical Prospecting*, *64*(4), 789–798.

Tao, G., King, M. S., & Nabi-Bidhendi, M. (1995). Ultrasonic wave propagation in dry and brine-saturated sandstones as a function of effective stress: Laboratory measurements and modelling1. *Geophysical Prospecting*, *43*(3), 299–327.

Tisato, N., & Madonna, C. (2012). Attenuation at low seismic frequencies in partially saturated rocks: Measurements and description of a new apparatus. *Journal of Applied Geophysics*, *86*, 44–53.

Tisato, N., Quintal, B., Chapman, S., Podladchikov, Y., & Burg, J.-P. (2015). Bubbles attenuate elastic waves at seismic frequencies: First experimental evidence. *Geophysical Research Letters*, *42*, 3880–3887. https://doi.org/10.1002/2015GL063538

Vajdova, V., Baud, P., & Wong, T. (2004). Compaction, dilatancy, and failure in porous carbonate rocks. *Journal of Geophysical Research*, *109*, B05204. https://doi.org/10.1029/2003JB002508

Walsh, J. B. (1965). The effect of cracks on the compressibility of rocks. *Journal of Geophysical Research*, *71*, 2591–2599.